CHARMM-Based Parameterization of Neutral Articaine—A Widely Used Local Anesthetic

ÉRICA T. PRATES,[1] PAULO C. T. SOUZA,[1] MÓNICA PICKHOLZ,[2] MUNIR S. SKAF[1]

[1]*Institute of Chemistry, State University of Campinas—UNICAMP, Campinas, SP 13084-862, Brazil*

[2]*Facultad de Farmacia y Bioquimica, Universidad de Buenos Aires, Buenos Aires, Argentina*

Received 9 December 2009; accepted 25 February 2010
Published online 9 September 2010 in Wiley Online Library (wileyonlinelibrary.com).
DOI 10.1002/qua.22701

ABSTRACT: We present a set of CHARMM-based parameters of molecular mechanics force field for neutral articaine (ATC), a potent and widely used local anesthetic in medical and dental applications. Partial atomic charges and effective torsion potentials around four chemical bonds, not available in CHARMM for this molecule, were obtained from quantum chemical calculations. The newly parameterized model was evaluated by examining the behavior of ATC in water and in a phospholipid bilayer using molecular dynamics simulations. ©2010 Wiley Periodicals, Inc. Int J Quantum Chem 111: 1339–1345, 2011

Key words: articaine; local anesthetics; CHARMM parameters; molecular dynamics

1. Introduction

Local anesthetics (LA) are compounds that can relieve and prevent pain by reversibly interrupting nerve conduction. As the name implies, these drugs act locally, anywhere in the nervous system, and in all types of nerve fibers. Typically, the structure of LA comprises a hydrophilic (an amine) and a hydrophobic (an aromatic ring, usually benzene) region, which are separated by an amide or ester linkage. Lidocaine and bupivacaine, for instance, which are among the most commonly used LA [1], are classified as amino amides, since the hydrophilic group is a tertiary amine and the linkage with the hydrophobic group (an aromatic ring) is an amide. Procaine, on the other hand, has an ester as intermediate group and is, therefore, classified as an amino ester LA [2, 3].

The anesthetic effect occurs because the LA molecules diffuse into the phospholipid membranes and cause conformational changes in the voltage-dependent sodium channel, leading to the temporary inactivation of this transmembrane

Correspondence to: M. S. Skaf; e-mail: skaf@iqm.unicamp.br
Contract grant sponsors: Brazilian Agencies Fapesp and CNPq.

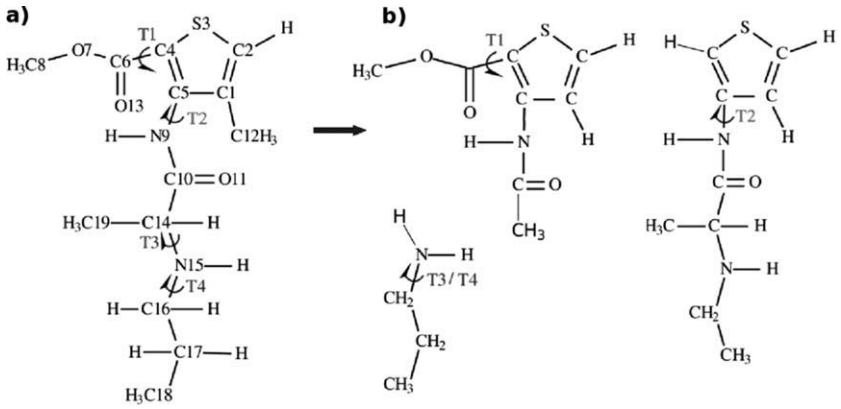

FIGURE 1. (a) Chemical formula of ATC, indicating atom numbering and the four parameterized torsions. (b) Simplified molecular structures used in the ab initio quantum chemical scans for each torsion.

protein and, consequently, the interruption of nerve transmission that causes the sensation of pain [4]. Aiming to improve the efficacy of these drugs and to reduce their side effects in humans by means of rational design of new LAs, many experimental studies have been dedicated to the understanding of the molecular mechanisms involved in the LA pharmacological effect [2, 5–17].

From a theoretical perspective, atomistic molecular dynamics (MD) computer simulations are being successfully applied to investigate the effects of various LAs on model phospholipidic membranes at a molecular level [18–23]. However, because of the wide variety of these compounds, it is often needed to develop new interaction potential parameters that allow the study of these systems by MD simulations.

Articaine (ATC) (Fig. 1) is a local anesthetic widely used in dermatological and dental applications that exhibits fast response times and low allergenicity [24], but whose action at the molecular level is, nevertheless, still poorly understood. ATC belongs to the LA class called amino amides and presents two very particular and unique features among the known LA: its aromatic portion consists of a thiophene ring instead of benzene and attached to the aromatic ring there is an ester group, which contributes to the rapid metabolism of the drug by enzymatic hydrolysis into articainic acid [24].

In this work, we develop force field parameters for computer simulations of articaine. We develop a set of molecular mechanics (MM) parameters for both stereoisomers of ATC, consistent with the well-known CHARMM force field for biomolecular systems [25] and use MD simulations to examine the behavior of the drug in aqueous solutions and in a palmitoyl-oleyl-phosphatidylcholine (POPC) phospholipid bilayer. For ATC in particular, there are CHARMM parameters available for the stretching of all bonds and angular distortions, as well as Lennard-Jones energy and distance parameters for all atomic types. However, because of the specificity of ATC's molecular structure and the lack of reasonably similar dihedrals readily available in CHARMM, torsional potentials for several dihedral angles (Fig. 1) were parameterized to adequately describe the conformational motions [26] of a flexible molecule such as ATC. By the same token, partial atomic charges were also parameterized.

2. Methods

2.1. PARAMETERIZATION OF THE ATC MOLECULE

In this work, we developed a set of parameters for ATC suitable for use within the CHARMM force field scheme [26]. Molecular geometry optimizations were performed at the density functional theory level with the B3LYP hybrid functional [27, 28] with basis set 6-311g(d,p) and a polarized continuum model (PCM) [29] with solvent dielectric constant of 80, corresponding to liquid water at ambient conditions, as implemented in the Gaussian03 molecular package [18]. The partial atomic charges for the two enantiomers R-articaine (R-ATC) and S-articaine (S-ATC) were obtained through a single point ab initio calculation at the RHF/6-31G(d) level using the

Merz-Singh-Kollman scheme [30]. The same level of theory was used determine selected torsional energy profiles [31, 32].

The CHARMM force field has the following functional form:

$$V = \sum_{\text{bonds}} K_b\left(r - r_{0,b}\right)^2 + \sum_{\text{angle}} K_a\left(\theta - \theta_{0,a}\right)^2 + \sum_{\text{UB}} K_{\text{UB}}\left(S - S_{0,\text{UB}}\right)^2 + \sum_{\text{dihedrals}} K_{d,n}\left(1 + \cos\left(n\chi - \delta_{d,n}\right)\right) + \sum_{\text{impropers}} K_i\left(\psi - \psi_{0,i}\right)^2 + \sum_{\text{nonbonded}} \varepsilon_{ij}\left[\left(\frac{R_{\min,ij}}{r_{ij}}\right)^{12} - 2\left(\frac{R_{\min,ij}}{r_{ij}}\right)^{6}\right] + \frac{q_i q_j}{4\pi\varepsilon_0 r_{ij}} \quad (1)$$

where the force constants K_b, K_a, K_{UB}, and K_i were obtained by analogy with similar groups available in CHARMM and the respective values of the equilibrium bond lengths and angles obtained from the quantum chemical calculations. The nonbonded van der Waals interactions are described by 12-6 Lennard-Jones pair potentials, with parameters for each atomic type completely transferred from CHARMM.

In devising force field parameters for intramolecular interactions, one typically attempts to reproduce the quantum potential energy surface with a set of effective analytical functions. In this case, all but the four selected dihedral torsional potentials are known. Therefore, we adjusted the missing torsion potentials in the full expression of the classical bonded interactions [first two lines in Eq. (1)] to fit the quantum energies as functions of the dihedral angles. The ab initio torsional energy maps for the four dihedral torsions were obtained from full 360° rotational scans taken at 15° steps. At each 15° dihedral angle increment, the molecular geometry was fully relaxed, keeping fixed the selected dihedral angle. The molecular mechanics energy for each molecular conformation was computed using the NAMD 2.7 package [33]). In this way, values for the $K_{d,n}$, $\delta_{d,n}$, and n parameters [see the fourth term of Eq. (1)] were obtained by the nonlinear curve fitting. Consistently with the CHARMM force field, these series were truncated in $n = 3$ and the phase angles were restricted to 0° or 180° [26].

ATC has an asymmetric carbon [C14 in Fig. 1(a)], which indicates optical activity through the right and left-handed R and S stereoisomers. All the procedure described here was carried out for the R isomer. However, since the conformations of stereoisomers at the energy minimum are mirror images of each other, the obtained parameters are readily transferable to the S isomer.

2.2. MOLECULAR DYNAMICS SIMULATIONS

To investigate the conformational behavior of the two ATC enantiomers in different environments, we have performed MD simulations of an ATC molecule in water, followed by simulations of ATC in a POPC lipid bilayer. We have used the TIP3P model for water [34], whereas the lipid molecules were described by CHARMM27 [32].

For the ATC in the aqueous environment, we performed 2 ns simulations after equilibration with a single ATC molecule immersed in a box of 1,100 water molecules in the *NpT* ensemble at 1 bar and 310 K. For the model biomembranes, five 20 ns simulations were carried out of the single ATC in a POPC phospholipid bilayer. The bilayer consisted of 126 POPC lipids hydrated by 4,580 water molecules. The simulations were performed using the Np_zAT ensemble, in which the number of molecules, normal pressure (1 bar), surface area (40.86 nm^2), and temperature (310 K) were kept constant. The fixed lateral area corresponds to the experimentally determined area per lipid of 65 $Å^2$ [35].

For all simulations reported here, Langevin dynamics and Nosé-Hoover Langevin piston methods [36, 37] were used to keep the temperature and the pressure constant. The RESPA multiple-time step algorithm [38] was used with the shortest time step of 2 fs. A cutoff of 10–12 Å was used for the Lennard-Jones interactions, whereas the long-range electrostatics forces were treated by means of the particle mesh Ewald (PME) technique [39]. All bonds involving hydrogen atoms were kept rigid using SHAKE [40].

3. Results and Discussion

3.1. PARAMETERS FOR ARTICAINE

Table I shows the atomic charges computed for ATC, according the atom numbering of Figure 1. The procedure to obtain the parameters for the dihedral potential, described in the previous

TABLE I

Atomic partial charges in atomic units obtained for ATC.

Atom	Charge (u.a.)	Atom	Charge (u.a.)
C1	0.026	H12	0.143
C2	−0.225	O13	−0.666
H2	0.239	C14	0.479
S3	0.002	H14	−0.004
C4	−0.656	N15	−0.935
C5	0.568	H15	0.379
C6	1.046	C16	−0.286
O7	−0.341	H16	−0.005
C8	−0.154	C17	0.071
H8	0.114	H17	0.018
N9	−0.603	C18	−0.342
H9	0.332	H18	0.082
C10	0.589	C19	−0.385
O11	−0.590	H19	0.092
C12	−0.438		

Atom numbering follows Figure 1(a). The hydrogen atoms are enumerated based on the number of the atom to which it is attached.

section, was carried out for the four selected torsions shown in Figure 1(a). For the other dihedral angles, the parameters were transferred from equivalent ones found in CHARMM force field parameterization of the c35b2 release. The results are depicted in Figure 2. To calculate the rotational energy barriers, the rotation angles could be described by different quartets of atoms. We have chosen the groups of atoms highlighted in Figure 2 and detailed in Table II. To diminish computational efforts, without compromising the essentials of the quantum chemical calculations as far as the rotational energies are concerned, we have divided the molecule into different parts and substituted longer side groups of the molecule by shorter surrogate fragments [Fig. 1(b)]. For computing the energy scans for the T1 dihedral torsion, for instance, we replaced the entire group of atoms bound to C14 by a methyl, maintaining the amide group and the aromatic ring intact, since they affect the electronic density in the T1 region by resonance.

The overall appearance of the QM and MM energy difference curves shown in Figure 2 reflects factors such as the hybridization of the atoms involved and electronic resonance. For instance, we can see from the difference curve for T1 that the minima are found in 0° and 180°. This planar conformation relative to the thiophene ring is consistent with the tendency of this group to withdraw electrons from the ring by resonance. The energy difference for T3, in contrast, has three minima, representing the sp^3 hybridization of the nitrogen. Not surprisingly, the results for the T4 torsion turned out very similar to that of the T3 dihedral and, therefore, we assumed the same torsion parameters for both of them.

The torsional potentials obtained for the dihedral angles defined by the atoms highlighted in Figure 2 describe the total dihedral angle potential for each bond rotation. However, the functional form of the CHARMM force field considers contributions from all dihedral angles that involve the torsion about a given bond. Therefore, we assumed the total constant $K_{d,n}$ equally divided among all the involved dihedral angles. Our best fitting parameters are shown in Table II, corresponding to the torsions T1, T2, and T3 (or T4) obtained by adjusting the data depicted in Figure 2. Additional information about bonded and nonbonded parameters and partial atomic charges are provided as Supporting Information.

To test the parameterized potential for ATC, we have performed a MM energy minimization of ATC in vacuum using a standard conjugated gradient algorithm [41] in NAMD and compared with the DFT/B3LYP/6-311g(d,p)/PCM

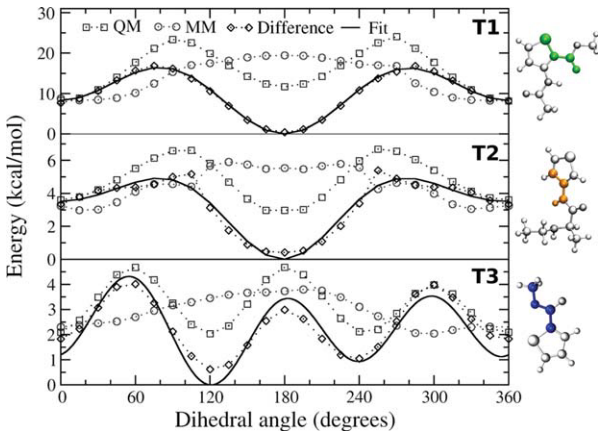

FIGURE 2. (a) Potential energy curves generated for the torsions T1, T2, and T3. The values of the potential energy computed by density functional theory are marked with squares (QM), whereas the corresponding values generated from the classical potential are marked with circles (MM). The QM and MM energy differences are depicted by diamonds and the solid lines are the fitted dihedral potentials. [Color figure can be viewed in the online issue, which is available at wileyonlinelibrary.com.]

TABLE II

Parameters of the torsional rotations T1, T2, and T3 determined by fitting the potential energy curves shown in Figure 2.

	Torsion	$K_{d,n}$ (kcal/mol)	n	$\delta_{d,n}$ (degrees)
T1	S3-C4-C6-O13[a]	1.250	1	180.0
		−1.110	2	0.0
		0.770	1	0.0
T2	C1-C5-N9-H9[a]	−0.780	2	0.0
		0.110	3	0.0
		−0.092	1	0.0
T3	C10-C14-N15-H15[a]	−0.042	2	180.0
		0.120	3	0.0

[a] The same values of $K_{d,n}$, n, and $\delta_{d,n}$ were assigned to different dihedral angles that define a given torsion.

optimized geometry. The optimized structures, shown in Figure 3(a), are practically indistinguishable, indicating that the MM force field reproduces the quantum chemical ground state molecular conformation of ATC in solution, consistent with previous studies which have shown that combining DFT with PCM provides reliable geometry estimates for small molecules in solution [42].

3.2. MD SIMULATIONS OF ATC IN DIFFERENT ENVIRONMENTS

First, we sampled the ATC conformational space in aqueous solution using MD simulations. Figure 3(b) depicts superposed molecular snapshots for ATC extracted at each 100 steps of the MD trajectory, along with the DFT optimized structure. The superposition was also carried out by completely aligning the rings [Fig. 3(c)]. In both figures, it is shown that the positions of the atoms fluctuate in the vicinity of the global minimum provided by the reference QM structure. The main changes are observed for the amine and carbon chain groups [atoms 14–19 in Fig. 1(a)], as expected, since there are only single bonds involved and no stabilization effects from electronic resonance.

The radial distribution functions between selected ATC atoms and water molecules (Fig. 4) reveal that curves for the pairs HW…O13, HW…O11, HW…N15, OW…H15, and OW…H9 show well-defined first peaks approximately located at 1.9 Å, typical of hydrogen (H)-bond interactions [43]. These results indicate that the partial charges and solute conformational features are capable producing H-bonds between ATC and water, with ATC acting both as an H-bond donor and acceptor, as expected on the basis of its electronic structure.

We have also carried out a series of simulations of ATC in a POPC lipid bilayer to examine the overall behavior of articaine in biomembranes. A single ATC molecule was originally placed in the aqueous phase. In three of these simulations, ATC was observed to diffuse spontaneously toward the interior the POPC lipid bilayer during the course of the simulations. Once in the interior of the bilayer, ATC was predominantly found in the vicinity of POPC's glycerol carbonyl group, roughly 8 Å away from the average position of the aqueous interface. This behavior is consistent with the fact that ATC, like many other LAs, is a hydrophobic molecule which has been experimentally found to penetrate biomembranes [44, 45]. In Figure 5, we compare the superposed MD snapshots of the ATC in water (left) and in the lipid bilayer (right). In aqueous solution, ATC clearly exhibits greater conformational freedom than in the interior of the POPC bilayer. The calculated average dipole moment of ATC turned out 4.0 ± 1.6 D and 2.6 ± 0.8 D in water and in POCP, respectively. A larger solute dipole moment in water is consistent with the higher polarity of the aqueous environment. Interestingly, there is a strong similarity between the structure that was optimized in vacuum (at classical or quantum levels) and the average structure of the ATC in the membrane. In fact, the average electric dipole moment of ATC in the membrane coincides with that of the optimized quantum structure of ATC.

Further studies of the interactions of ATC with POPC bilayers are currently in progress using the parameters reported here. Our results for several physicochemical properties of ATC in POPC membranes are in excellent agreement with

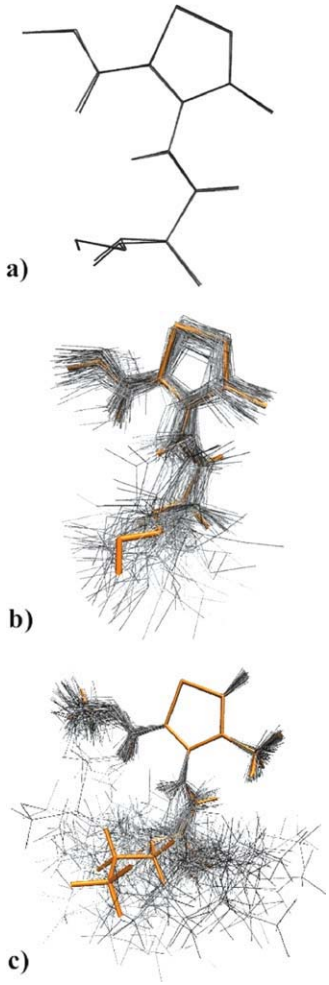

FIGURE 3. (a) Superposition of the MM and DFT/PCM minimized structures. (b) Superposition of the ATC structures extracted from the aqueous solution simulations together with the DFT/PCM optimized geometry (thicker, orange traces). (c) Same as (b), but with the aromatic ring alignment. [Color figure can be viewed in the online issue, which is available at wileyonlinelibrary.com.]

experiments and shall be published separately. Together with the results presented here, this suggests that the model proposed for the ATC is suitable for computer simulations of this compound in a variety of systems.

4. Concluding Remarks

In this work, we developed a set of parameters committed to the CHARMM force field suitable for molecular simulations of neutral articaine, the most potent form of this important local anesthetic. The study focuses specially on the parameterization of dihedral torsion potentials and partial atomic charges. The newly parameterized model reproduces very well the quantum mechanical ground state molecular conformation of ATC in vacuum. Molecular dynamics simulations of ATC in aqueous solution using the proposed potential show that the model is well-behaved in the sense that ATC is capable of H-bonding to water as bond acceptor and donor and its molecular conformations fluctuate around the optimized geometry. The relative mobility of different parts of the molecule reflects appropriately torsional features impacted by factors such as electronic resonance and the flexibility of the aliphatic chain. As a result, the average electric dipole moment of ATC in water increases by roughly 60% relative to the gas phase value, indicating ATC's ability to polarize in a high dielectric constant environment.

Simulations of ATC in model phospholipid bilayers show that the drug diffuses from the

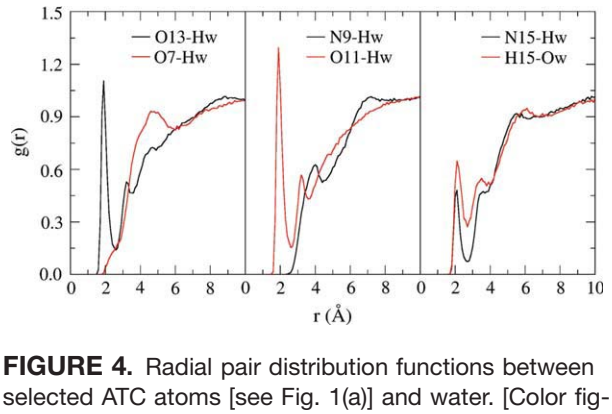

FIGURE 4. Radial pair distribution functions between selected ATC atoms [see Fig. 1(a)] and water. [Color figure can be viewed in the online issue, which is available at wileyonlinelibrary.com.]

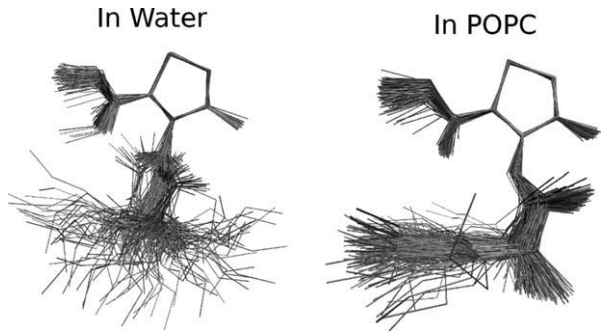

FIGURE 5. Superposed snapshots of ATC in water (left) and in the POPC membrane (right).

aqueous environment to the interior of the membrane and maintains a stable position there. That agrees very well with the proposal of the role of membrane on modulating the LA access to the voltage-dependent sodium channel. In the membrane, ATC exhibit a preferential U-shaped average conformation which is very similar to the optimized structure in vacuum and presents the same value of electric dipole moment.

The proposed CHARMM-like set of parameters for ATC has been shown suitable for MD and other molecular simulations studies of ATC in aqueous solutions and in phospholipidic biomembranes.

ACKNOWLEDGMENT

E.P. and P.S. gratefully acknowledge Fapesp for graduate fellowships.

References

1. Malamed, S. F.; Gagnon, S.; Leblanc, D. J Am Dent Assoc 2001, 132, 177.
2. Araujo, D. R.; de Paula, E.; Fraceto, L. F. Quim Nova 2008, 31, 1775.
3. Covino, B. G.; Vassalo, H. G. Local Anesthetics: Mechanisms of Action and Clinical Use; Grune and Stratton: New York, 1976.
4. Butterworth, J. F.; Strichartz, G. R. Anesthesiology 1990, 72, 711.
5. Strichartz, G. R.; Ritchie, J. M. In Local Anesthetics: Handbook of Experimental Pharmacology; Strichartz, G. R., Ed.; Springer-Verlag: Berlin, 1987; Vol. 81, p 21.
6. de Paula, E.; Schreier, S. Braz J Med Res 1996, 29, 877.
7. Arias, H. R. Biochim Biophys Acta 1998, 1376, 173.
8. Slater, J. S.; Kelly, M. B.; Larkin, J. D.; Ho, C.; Mazurek, A.; Taddeo, F. J.; Yeager, M. D.; Stubs, C. D. J Biol Chem 1977, 272, 6167.
9. Kalipatnapu, S.; Chattopadhyay, A. Cell Mol Neurobiol 2004, 24, 403.
10. Hirata, M.; Sakaguchi, M.; Mochida, C.; Sotozono, C.; Kageyama, K.; Kuroda, Y.; Hirose, M. Anesthesiology 2004, 100, 1026.
11. Cohen, S. P.; Mao, J. Acta Anesthesiol Scand 2003, 47, 910.
12. Hodgkin, A. L.; Huxley, A. F. Physiology 1952, 117, 500.
13. Narahashi, T.; Yamada, M. Nature 1969, 223, 748.
14. Frazier, D. T.; Narahashi, T.; Yamada, M. J Pharmacol Exp Ther 1970, 171, 45.
15. Ragsdale, D. S.; McPhee, J. C.; Scheuer, T.; Catterall, W. A. Science 1994, 265, 1724.
16. Ragsdale, D. S.; McPhee, J. C.; Scheuer, R.; Catterall, W. A. Proc Natl Acad Sci USA 1996, 93, 9270.
17. Lee, A. G. Biochim Biophys Acta 1976, 448, 34.
18. Vemperala, S.; Saiz, L.; Eckenhoff, R. G.; Klein, M. L. Biophys J 2006, 91, 2815.
19. Pickholz, M.; Oliveira, O. N.; Skaf, M. S. J Phys Chem B 2006, 110, 8804.
20. Pickholz, M.; Oliveira, O. N.; Skaf, M. S. Biophys Chem 2007, 125, 425.
21. Cabeça, L.; Pickholz, M.; de Paula, E.; Marsaioli, A. J Phys Chem B 2009, 113, 2365.
22. Högberg, C. J.; Maliniak, A.; Lyubartsev, A. Biophys Chem 2007, 125, 416.
23. Högberg, C. J.; Lyubartsev, A. P. Biophys J 2008, 94, 525.
24. Jacob, S. E.; Patel, A. R. Dermatol Surg 2007, 33, 256.
25. Brooks, B. R.; Brooks, C. L., III; Mackerell, A. D., Jr.; Nilsson, L.; Petrella, R. J.; Roux, B.; Won, Y.; Archontis, G.; Bartels, C.; Boresch, S.; Caflisch, A.; Caves, L.; Cui, Q.; Dinner, A. R.; Feig, M.; Fischer, S.; Gao, J.; Hodoscek, M.; Im, W.; Kuczera, K.; Lazaridis, T.; Ma, J.; Ovchinnikov, V.; Paci, E.; Pastor, R. W.; Post, C. B.; Pu, J. Z.; Schaefer, M.; Tidor, B.; Venable, R. M.; Woodcock, H. L.; Wu, X.; Yang, W.; York, D. M.; Karplus, M. J Comput Chem 2009, 30, 1545.
26. Guvench, O.; MacKerell, A. D., Jr. J Mol Model 2008, 14, 667.
27. (a) Becke, A. D. J Chem Phys 1993, 98, 5648; (b) Lee, C.; Yang, W.; Parr, R. G. Phys Rev B 1988, 37, 785.
28. Stephens, P. J.; Devlin, F. J.; Chabalowski, C. F.; Frisch, M. J. J Phys Chem 1994, 98, 11623.
29. Kim, K.; Jordan, K. D. J Phys Chem 1994, 98, 10089.
30. Singh, U. C.; Kollman, P. A. J Comput Chem 1984, 5, 129.
31. MacKerell, A. D., Jr.; Feig, M.; Brooks, C. L. J Comput Chem 2004, 25, 1400.
32. Feller, S. E.; Gawrisch, G.; MacKerell, A. D., Jr. J Am Chem Soc 2002, 124, 318.
33. Phillips, J. C.; Braun, R.; Wang, W.; Gumbart, J.; Tajkhorshid, E.; Villa, E.; Chipot, C.; Skeel, R. D.; Kale, L.; Schulten, K. J Comput Chem 2005, 26, 1781.
34. Jorgensen, W. L.; Chandrasekhar, J.; Madura, J. D. J Chem Phys 1983, 79, 926.
35. Lantzsch, G.; Binder, H.; Heerklotz, H. J Fluoresc 1994, 4, 339.
36. Schneider, T.; Stoll, E. Phys Rev B 1978, 17, 1302.
37. (a) Martyna, G. J.; Tobias, D. J.; Klein, M. L. J Chem Phys 1994, 101, 4177; (b) Feller, S. E.; Zhang, Y.; Pastor, R. W.; Brooks, B. R. J Chem Phys 1995, 103, 4613.
38. Tuckerman, M. E.; Berne, B. J.; Martyna, G. J. J Chem Phys 1992, 97, 1990.
39. Darden, T.; York, D.; Pedersen, L. J. J Chem Phys 1993, 98, 10089.
40. Ryckaert, J. P.; Ciccotti, G.; Berendsen, H. J. C. J Comput Phys 1977, 23, 327.
41. (a) Hestenes, M. R.; Stiefel, E. J. Res Nat Bur Stand 1952, 49, 409; (b) Fletcher, R.; Reeves, C. M. Comput J 1964, 7, 149.
42. Branca, M.; Alezra, V.; Kouklovsky, C.; Archirel, P. Tetrahedron 2008, 64, 1743.
43. Ladanyi, B. M.; Skaf, M. S. Annu Rev Phys Chem 1993, 44, 335.
44. Song, C.; Lygre, H.; Nerdal, W. Eur J Pharm Sci 2008, 33, 399.
45. Lygre, H.; Moe, G.; Nerdal, W.; Holmsen, H. Acta Odont Scand 2009, 67, 1.